Atmospheric Environment 191 (2018) 142–152

Contents lists available at ScienceDirect

Atmospheric Environment

journal homepage: www.elsevier.com/locate/atmosenv

Estimating daily and intra-daily PM_{10} and $PM_{2.5}$ in Israel using a spatio-temporal hybrid modeling approach

Alexandra Shtein[a,*], Arnon Karnieli[b], Itzhak Katra[a], Raanan Raz[c], Ilan Levy[d], Alexei Lyapustin[e], Michael Dorman[a], David M. Broday[f], Itai Kloog[a]

[a] Department of Geography and Environmental Development, Ben-Gurion University of the Negev, Beer Sheva, Israel
[b] Jacob Blaustein Institutes for Desert Research, Ben-Gurion University of the Negev, Sede Boker Campus, 84990, Israel
[c] Braun School of Public Health and Community Medicine, The Hebrew University of Jerusalem, Jerusalem, Israel
[d] Israel Ministry of Environmental Protection, Tel-Aviv, Israel
[e] National Aeronautics and Space Administration (NASA) Goddard Space Flight Center (GSFC), Code 613, Greenbelt, MD, USA
[f] Civil and Environmental Engineering, Technion, Haifa, Israel

ARTICLE INFO

Keywords:
Air pollution
PM_{10}
$PM_{2.5}$
Intra-daily estimation
Aerosol optical depth (AOD)
MAIAC

ABSTRACT

Satellite-based particulate matter (PM) models provide spatially and temporally resolved estimations, allowing greater spatial-temporal coverage compared to sparse ground monitoring stations. The spatio-temporal resolution of these models can be improved using aerosol optical depth (AOD) products from various satellite platforms with different overpass times which can capture possible changes in diurnal aerosol concentrations. Israel is characterized by diverse geo-climatic regions and it is subjected to frequent dust storms events. Our goal was to estimate PM_{10} and $PM_{2.5}$ concentrations in Israel on daily and intra-daily (mean PM around the Aqua and Terra overpasses) temporal resolutions and to assess the differences between these time windows. A hybrid modeling approach that consists of three stages was used enabling spatially continuous PM estimations at 1 × 1 km spatial resolution. The model was calibrated on a daily basis applying a mixed modeling approach using MODIS-based MAIAC AOD and various spatial and temporal predictors. It was found that in certain urban areas the measured and estimated PM concentrations during the satellite overpass (Terra or Aqua) were higher than the mean daily PM. The models performed well showing cross-validated R^2 that ranged between 0.82 and 0.92. Mean estimated PM for the study period (2005–2015) during days with no dust events showed different spatial patterns for the daily and intra-daily estimations and revealed areas in Israel that are affected by high PM concentrations (mainly industrial or dense urban areas). Estimations from these models are useful for epidemiological research and might contribute to environmental regulatory purposes by focusing the efforts of PM pollution reduction at the identified polluted areas.

1. Introduction

Particulate matter (PM) is one of the regularly monitored air pollutants due to its substantial effect on human health. Exposure to PM is linked to various health outcomes such as respiratory disease (Dominici et al., 2006; Kloog et al., 2013, 2012a; Kurt et al., 2013; Schwartz, 1995), cardiovascular disease (D'Ippoliti et al., 2003; Dominici et al., 2006; Hartog et al., 2009; Madrigano et al., 2013; Rich et al., 2013; Zanobetti and Schwartz, 2005), and pregnancy outcomes (Bell et al., 2007; Kloog et al., 2012b; Zeka et al., 2008). High PM levels can be attributed to anthropogenic activities (transportation, industry, waste burning, and power plant emissions) and also to the occurrence of different natural events (dust storms, volcanic eruptions, sea spray, wildfires). Throughout the years, different models were established for assessing air pollution exposures (Jerrett et al., 2005). The outputs of such models were used for evaluating the association between exposure to air pollutants and various health outcomes (Sorek-hamer et al., 2016). Some of these models provided PM concentrations with high-temporal resolution (daily and hourly), however they were based on measurements from sparse ground instruments (Li et al., 2017; Zikova et al., 2017) or provided PM estimations with a spatial resolution of 3/10 km (Gupta and Christopher, 2008; You et al., 2016). Epidemiological studies might benefit from a modeling approach that will allow improved PM estimation, with high temporal and spatial resolution. The satellite-based hybrid modeling approach that was applied in various regions by different groups (Chudnovsky et al., 2014; de Hoogh et al.,

* Corresponding author.
E-mail address: shtien@post.bgu.ac.il (A. Shtein).

https://doi.org/10.1016/j.atmosenv.2018.08.002
Received 13 June 2018; Received in revised form 30 July 2018; Accepted 3 August 2018
Available online 04 August 2018

2018; Hu et al., 2014; Kloog et al., 2015; Lee et al., 2015; Stafoggia et al., 2016) showed good ability to estimate daily PM concentrations with cross validated R^2 ranging between 0.65 and 0.88 depending on the modelled area. These models apply statistical approaches that use satellite aerosol optical depth (AOD) data along with various meteorological and spatial predictors in a mixed effects modeling framework.

The Moderate Resolution Imaging Spectroradiometer (MODIS) sensor is located onboard two satellite platforms (Aqua and Terra), which differ in their overpass time (~3 h apart). Previous hybrid models (Chudnovsky et al., 2014; de Hoogh et al., 2018; Hu et al., 2014; Kloog et al., 2015; Lee et al., 2015; Stafoggia et al., 2016) that were applied in different regions used MODIS-based AOD data retrieved from the Multi Angle Implementation of Atmospheric Correction (MAIAC) algorithm. Specifically, the 1 × 1 km MAIAC AOD product from the Terra platform is available over Israel between 09:00–12:40 Israel Standard Time (IST), and from the Aqua platform between 11:10–15:00 IST. It is generally assumed that different times of the day may be characterized by different PM concentrations due to variability in the factors that influence air pollutants levels, such as human activity (industry and transportation), synoptic conditions (Uzan et al., 2012), air mass properties (e.g. height, density, velocity) (Kok, 2011), and dust emission from local and remote sources (Freiman et al., 2006; Krasnov et al., 2016b).

In mid-winter, typical episodes of high anthropogenic air pollution occur when pollutants are trapped in the lower atmospheric boundary layer due to the formation of near-surface temperature inversion during favorable synoptic conditions (Derimian et al., 2006). Uzan et al. (2012) showed that the lowering of the mixing layer height during the summer period in the Israeli coastal area lead to high air pollution events due to the trapping of locally emitted pollutants during certain times of the day. More specifically, Karnieli et al. (2009) showed that the summer synoptic conditions cause long-range transport of pollution species to the region, particularly sulfur from southeastern and southwestern Europe.

Israel is also substantially affected by natural mineral dust storms that transport windblown dust particles from remote locations (Ganor et al., 2009; Katra et al., 2014; Yuval et al., 2015), alongside the contribution of dust from local sources of eroded soils (Katra et al., 2016). Particles from these different sources (natural versus anthropogenic) are characterized by different chemical composition and size distribution (Falkovich, 2004), and therefore their effect on human health can vary. Estimation of PM during different times of the day might express the diurnal variability and allow better assessment of PM exposure.

To the best of our knowledge, this is the first work estimating intra-daily spatially continuous PM concentrations using satellite data in Israel. These estimations are useful for epidemiological studies as they may be used to examine the effect of PM on health outcomes in different hours of the day that possibly originate from different sources, rather than using a 24-hours mean PM estimates. The primary goal of the study was to estimate PM_{10} and $PM_{2.5}$ concentrations in Israel on daily (24-hours mean PM) and intra-daily (mean PM around the Aqua and Terra overpasses) temporal resolutions. This was achieved using a hybrid three stage modeling approach which applies a mixed modeling framework in each stage. The specific objectives of this research were: (1) Compare the PM concentrations and the mean spatial patterns of the estimations from different time windows. (2) Compare the performance of intra-daily models that use hourly specific AOD for estimating PM around the satellite overpass with the performance of daily models that use hourly AOD to estimate daily mean PM concentrations.

2. Material and methods

2.1. Study domain

The study area contains the State of Israel (Fig. 1), apart from regions that either do not contain reliable and available air monitoring data, or the population there is very scarce. The potential use of the estimations from the proposed model for epidemiological studies led to delineation of the research area to the more populated regions in Israel. Israel is located along the southeastern shore of the Mediterranean Sea (between 34.2 and 35.9ºE and 29.5–33.4ºN). The Israeli climate is characterized by winter rains occurring mainly during November through March, and a relatively long, dry, and hot summer. Its proximity to the global dust belt, which extends from West Africa to the Arabian Desert, influences the PM concentration levels substantially due to dust storms that occur mainly during the winter and transition seasons (Derimian et al., 2006; Ganor et al., 2009; Krasnov et al., 2014; Yuval et al., 2015). Despite its small area (~420 km from north to south and a maximum width of ~110 km), Israel experiences sharp climatic gradient, from arid climate in the south, through semi-arid climate in the center, and up to Mediterranean climate in the northern parts. Israel is also characterized by a variety of geographical areas such as: large rural areas, large forested regions, water bodies, mountains, and the Mediterranean coastal plains.

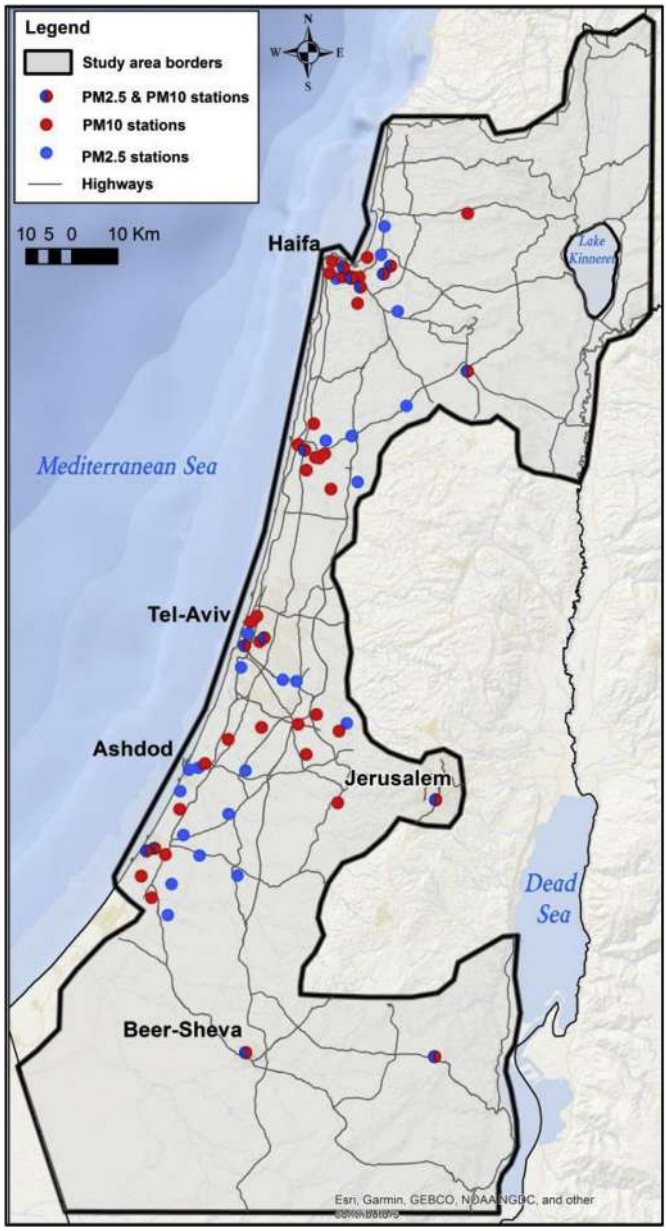

Fig. 1. The study area (delimited by black line) and the PM_{10} and $PM_{2.5}$ monitoring stations that were included in the model.

2.2. Ground monitoring data

The PM ground monitors in Israel are distributed mainly in the coastal populated area and within its major cities (Tel Aviv, Jerusalem, Haifa, Ashdod, and Beer-Sheva) (Fig. 1). Quality assured $PM_{2.5}$ and PM_{10} concentrations in half hourly temporal resolution across Israel for the years 2005–2015 were obtained from the Technion Center of Excellence in Exposure Science and Environmental Health (TCEEH) air pollution monitoring database. Daily (24-hours) and intra-daily (around the overpass time of Terra and Aqua) mean PM concentrations were calculated as the mean of the half-hourly PM concentrations. Air quality monitoring in Israel is conducted by different organizations and regulated by the Ministry of Environmental Protection (MOEP) (MEP, 2018). The measurements are performed using Tapered-Element Oscillating Microbalance (TEOM) monitoring instruments that are operated and maintained according to the United States Environmental Protection Agency (US-EPA) guidelines, with a typical accuracy of ± 5% (EPA, 2017). Overall, the model was based on data from 37 $PM_{2.5}$ air quality monitoring (AQM) stations and from 45 PM_{10} AQM stations that were operated during the study period.

2.3. Satellite data

AOD is one of the widely-used satellite based product for PM modeling. The AOD measures light extinction at given wavelengths due to aerosol and gaseous compounds scattering absorption along the measured atmospheric column, therefore making it useful for estimating PM concentrations. The AOD product is available from several algorithms of the MODIS sensor (Deep blue, Dark target, MAIAC), onboard the two satellite platforms (Terra and Aqua). The latest developed MAIAC algorithm was recently used in various locations for PM estimation (Arvani et al., 2016; de Hoogh et al., 2018; Just et al., 2015; Kloog et al., 2015; Stafoggia et al., 2016), due to its advantages for PM modeling including relatively high spatial resolution of 1 km, long time coverage (2000 - present for Terra and 2003 - present for Aqua), and improved accuracy over bright surfaces. Daily MAIAC AOD was retrieved from Terra and Aqua Collection 6 data for the period of 2005–2015. This time period was chosen due to the higher availability of PM monitoring stations and dust events classification data. Additional details about the MAIAC product and algorithm can be found in previous publications (Lyapustin et al., 2011a, 2011b). The AOD data may include some spurious values due to proximity to clouds, water bodies or measurement over very bright surfaces. Such values were removed from the database using quality assurance and uncertainty information metrics provided with the MAIAC AOD product.

2.4. Spatial and temporal predictors of $PM_{2.5}$ and PM_{10}

Alongside the satellite observations, the contribution of different spatial and temporal predictors to the hybrid model was evaluated. Within the linear mixed effect modeling framework, the effect of these predictors was considered as fixed effect terms. Sections 2.4.1 and 2.4.2 describe the spatial and temporal predictors, which were generated using R statistical software ver. 3.4.3 (R Core Team, 2017) and ArcMap ver. 10.4 (ESRI, 2018).

2.4.1. Spatial predictors

All spatial predictors were generated and assigned to the 1 × 1 km grid cell using the ArcGIS program (ESRI, 2018). Raster based predictors (land-use, population density, NDVI, elevation, roads density) were assigned to the 1 × 1 km grid cell using zonal statistics tool that allows calculating the mean raster values for each grid cell.

Population and land-use data were obtained from the Israeli Central Bureau of Statistics (ICBS, 2016). Population density in each tract was calculated and the weight averaged population density was assigned to each 1 × 1 km grid cell that is contained within the tract polygon. Land-use data were used to calculate the percentage of different land-uses in each 1 × 1 km grid cell across the study area. For 2005–2008 years a land use data-base updated for 2004 was used, while for 2009–2015 a land use data-base updated for 2014 was used. Four main groups of land-uses were defined: industrial, urban, agricultural, and open space.

Elevation data with a 30-m spatial resolution were obtained from the Advanced Spaceborne Thermal Emission and Reflection Radiometer (ASTER) global digital elevation model (GDEM) database (ASTER, 2014). The mean elevation was calculated and assigned to each 1 × 1 km grid cell.

Normalized Difference Vegetation Index (NDVI) data were retrieved from the publicly available monthly MODIS NDVI product (MOD13A3) at 1-km spatial resolution and assigned to each 1 × 1 km grid cell. Additional database of NDVI was created using the red and NIR bands of Landsat 7 & 8 at 30 m spatial resolution, and a the seasonal average NDVI in the summer and the spring was created. This improved database was used for the local stage of the model.

Several transportation (roads and railways) predictors were generated in order to assess their association with local PM levels. Road and railways data were obtained from the geographic information systems (GIS) vector layers of the 2012 road network (GISrael database of MAPA, 2012) and included all the roads across Israel. The types of roads (highways and major roads) were classified according to the methodology described in Levy et al. (2015). Based on these data several predictors were calculated and their averaged means in each 1 × 1 km grid cell were assigned to the grid cell: (1) total road density raster was created using the line density tool that calculates the density of polyline features (all the roads) that contained in 1-km radius around each 1-km cell centroid. (2) distance from major roads to the grid cell center, (3) distance from highways to the grid cell center, and (4) distance from the nearest railway to the grid cell center.

Distances to water bodies (Mediterranean Sea, Lake Kinneret (Sea of Galilee), and the Dead Sea were calculated from the centroids of the grid cell using ArcGIS and assigned to each cell.

2.4.2. Temporal predictors

Meteorological data and pollution monitoring data were obtained through the TCEEH air pollution monitoring database. Grid cells were matched to the mean of the nine closest weather stations with available meteorological variables. The following variables were extracted from this database and averaged daily and around the overpass time of the Terra and Aqua platforms: air temperature, relative humidity, wind speed, rainfall and Nitrogen Oxides (NOx) concentrations.

Dust day classification was used as a predictor in our model. Half-hourly Dust events classification data were used from the study of Yuval et al. (2015). For each AQM PM monitor, dust events classification was attributed from the closest available PM monitor. Each daily and intra-daily time windows were classified either as a dust day (if a dust event occurred at least once during that time period) or as non-dust days (if no dust events occurred). The frequency of dust days on a daily scale for each year is presented in the electronic Supplementary Material in Fig. A.1. This classification (dust or non-dust day) did not consider the duration of the dust event and its intensity. Although the model was ran for all days (dust and non-dust) together, the mean square error of the model was evaluated separately for dust and non-dust days.

The dispersion of pollutants depends on many meteorological parameters and the mixing height, or boundary layer depth, is one of the parameters that define the volume of air through which the pollution is mixed. The planetary boundary layer (PBL) can vary with the wind speed and can influence the concentration and the pollutant vertical profile (Oke, 1987). PBL height was obtained from modeled

data of the European Centre for Medium-Range Weather Forecasts (ECMWF, 2016) at a spatial resolution of approximately 13.9 km temporal resolution of 3-hours. In each day the corresponding PBL measurement (daily mean or measurement around Terra/Aqua overpass) was assigned to the 1 km grid cells.

2.5. Statistical methods

2.5.1. Modeling stages

All modeling stages were developed and run in R software (R, 2017). Three estimation models were developed for $PM_{2.5}$ and PM_{10}, each for a different time window: (1) Daily (24-hours mean, from 00:00 to 23:59 IST) model that uses the Aqua AOD product similarly to previous studies (e.g. Just et al., 2015; Kloog et al., 2015) that used this product; (2) Intra-daily (hourly) model that estimates PM around the Aqua overpass. This model uses Aqua AOD product as one of the predictors. The mean overpass of the Aqua satellite over Israel is 13:05 IST and the standard deviation is 1 h. Hence, this model estimates the mean PM between 10:00–16:00 IST; (3) Intra-daily (hourly) model that estimates PM around the Terra overpass. This model uses Terra AOD product as one of the predictors. The mean overpass of the Terra satellite over Israel is 10:50 IST, and the standard deviation is 1.5 h. Hence, this model estimates the mean PM between 08:00–14:00 IST. The wide time window used for the intra-daily models was chosen after evaluating the sensitivity of the model to different time window widths. A model that estimated PM on the specific satellite overpass time showed lower performance than models that estimated the mean PM over larger time periods. The length of the satellite-specific time window was chosen according to the range of overpass hours that was extracted from the metadata of the MAIAC AOD Hierarchical Data Format (HDF) files (Fig. 2) with one extra hour on each side of the time window (08:00–14:00 IST for Terra and 10:00–16:00 IST for Aqua).

In Israel, there is a day-to-day variability in PM concentrations and in different meteorological measurements (temperature, PBL, humidity, precipitation). These daily differences create also varying relationship between the PM and the AOD measurements. Therefore, mixed effects modeling was chosen to account for the temporal variations in the PM-AOD relationship by incorporating various spatial and temporal predictors and day-specific random-effects. The modeling approach consists of three main stages that allow estimation of PM concentration in every 1 × 1 km grid cell in each day. The first stage calibrates the AOD grid-level observations to the $PM_{2.5}$ or PM_{10} AQM stations using all monitor-day observations with the closest available AOD value within 1.1 km during the study period, while adjusting for spatial and temporal predictors. Specifically, the following linear mixed effects model (calibration stage) was fitted using the lmer4 package (Bates et al., 2015):

$$PM_{ijt} = (\alpha + u_j) + (\beta_1 + v_j)AOD_{ij} + \sum_{m=1}^{12} \gamma_{1m}X_{1mi} + \sum_{m=1}^{10} \gamma_{2m}X_{2mijt} + \varepsilon_{ij} \quad (1)$$

where PM_{ijt} is the measured PM_{10} or $PM_{2.5}$ concentrations at site i on day j, in reference to a certain time window t (daily/morning/afternoon); α and uj are the fixed and random (day-specific) intercepts, respectively; AOD_{ij} is the AOD value in the grid cell corresponding to site i on day j; and $\beta 1$ and vj are the fixed and day-specific random slopes, respectively. X_{1mi} is the value of the m-th spatial predictor at site i (i.e. population density, percent of certain land-use type, distance to the nearest main road, and elevation) and γ_{1m} is the corresponding fixed-effects slope of m-th spatial predictor. X_{2mijt} is the value of the m-th temporal predictor at site i, on day j (i.e. PBL height, NDVI, ambient temperature, relative humidity, NO_x concentrations, and dust classification) within the relevant time window t (daily/Terra overpass/Aqua overpass) and γ_{2m} is the corresponding fixed-effects slope of m-th temporal predictor.

After calibrating the model, the residuals of the first modeling stage were calculated (observed – predicted) and an additional, local, modeling stage was applied. The local stage aimed to improve the model performance locally, by fitting the residuals of the previous modeling stage to a model that accounts for higher resolution (200 m) spatial variables (NDVI, elevation, distance to roads, and percent of certain land-use type). The output of this stage is suitable when the model estimations are used for exposure assessment using address-specific geocoded data that is common in recent epidemiology studies. When detailed addresses data are not available, and exposure is based on small area (zipcode, census tract, etc.) or city level data, the 1 × 1 km

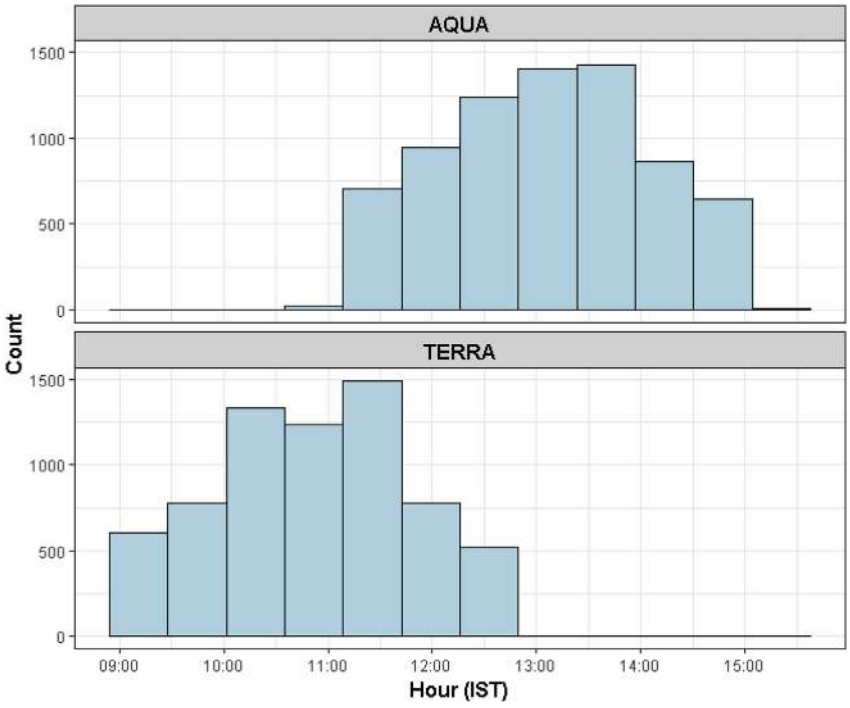

Fig. 2. Histogram of the overpass hours of Aqua and Terra satellites over Israel. The range of overpass hours is 09:00–13:00 for Terra and 11:00–15:00 for Aqua.

Table 1
Summary statistics of PM_{10} and $PM_{2.5}$ concentrations (μg/m^3) measured in air quality monitoring stations, located in four major cities in Israel, for the period of 2005–2015. Abbreviations: n- Number of stations, D- Daily average, H_A- Mean PM around the Aqua overpass, H_T- Mean PM around the Terra overpass, IQR-inter quartile range.

City	Model	PM_{10}				$PM_{2.5}$			
		Median	Mean	Max.	IQR	Median	Mean	Max.	IQR
Haifa	D	32	44	2153	22	16	18	1166	22
(n = 10)	H_A	34	49	2153	27	16	19	524	11
	H_T	34	48	2313	27	16	19	870	11
Tel-Aviv	D	41	57	1759	25	20	23	372	25
(n = 4)	H_A	39	58	2823	28	18	21	419	11
	H_T	43	60	2760	30	20	23	542	12
Jerusalem	D	36	53	2937	25	15	20	846	25
(n = 1)	H_A	39	57	4889	27	16	21	1347	9
	H_T	35	52	6290	26	14	18	1855	9
Beer-Sheva	D	38	56	3223	25	21	24	370	25
(n = 1)	H_A	39	63	2919	29	21	25	381	13
	H_T	38	56	2950	27	21	24	296	12

PM estimations are used without applying this stage.

The highly-resolved spatial predictors around each monitoring station were regressed against the residuals of the cross-validated stage 1 model using the support vector regression (SVR) methodology applied by the e1071 package (Meyer et al., 2017).

$$ResidPM_{ij} = \sum_{m=1}^{8} \alpha_m K(X_{mij}, x) + \varepsilon_{ij} \quad (2)$$

where $ResidPM_{ij}$ is the residual of $PM_{2.5}$ or PM_{10} concentration in site i and day j from the cross-validated phase 1 calibrated model; X_{mij} is the m-th spatial predictor around monitoring station i on day j; K is a kernel function which captures nonlinearities and interactions among the predictors of $ResidPM_{ij}$ and its parameters are chosen using 10-fold cross validation (CV).

The second stage PM estimation can be applied in locations where AOD retrievals exist using the calibration stage model coefficients. This stage resulted in PM estimation for all day-grid cell combinations with available satellite based AOD.

The third stage modeling phase estimates the PM concentrations in locations where there are no satellite based AOD observations. This stage is implemented by modeling the relationships between the estimated PM from stage 2 and the PM value from an inverse distance weighting (IDW) interpolation of PM observations from AQM stations each day, accounting for possible variability of the relationships in space, using the mixed modeling approach:

$$PredPM_{ij} = (\alpha + u_i) + (\beta_1 + v_i) * I_{PMij} + \varepsilon_{ij} \quad (3)$$

where $PredPMij$ is the predicted PM_{10} or $PM_{2.5}$ concentrations at grid cell i on day j based on the calibrated stage 1 model (i.e. predicted PM in grid points for which AOD is available); I_{PMij} is the PM derived from the IDW interpolation surface for site i on day j; α and u_i are the fixed and grid-cell specific random intercepts, respectively; and β_1 and v_i are the fixed and random slopes, respectively.

2.5.2. Model performance

Model performance was assessed using the ten-fold out-of-sample CV technique. The data were randomly divided into 90% training and 10% test datasets ten times. Each time, the model was trained based on 90% of the data, and a prediction of PM was made for the 10% out of sample data. To test the results for bias, the measured PM values were regressed in each site and day against the corresponding predicted values from the 90% sample. The CV technique was used to avoid model over-fitting, and for selecting the best combination of predictors for the model. The fixed effects in the calibration stage of the model were selected by backward selection using the fitLMER.fnc from the LMER Convenience Functions package (Tremblay and Ransijn, 2015) that used Akaike Information Criterion (AIC) estimator. The following model performance measures were calculated based on the CV results:

- Coefficient of determination (R^2) - the observed and predicted PM values were regressed, and the percent of explained variance was computed.
- Root mean standard error (RMSE) - the square root of the mean quadratic differences between observed and predicted PM values. It is a summary measure of the prediction error, and it is on the same scale as the measured observation (PM, μg/m^3).
- Slope - the coefficient from the linear regression between PM observed and PM predicted.
- Temporal R^2 - the whole study period predicted and observed averages were subtracted from the daily observed and the predicted series of PM concentrations. The daily observed and predicted PM deviations (i.e. the residuals after subtraction of the mean) were regressed against each other, and the R^2 coefficient was computed. This measure represents the contribution of the temporal variation to the total variance of the daily PM model predictions across all monitoring stations and days.
- Spatial R^2 - the daily average observed and predicted PM concentrations were averaged in each grid cell over the entire study period (2005–2015). The study-period average observed and predicted PM values in each grid cell were regressed against each other, and the R^2 coefficient was computed. This measure represents the contribution of the spatial variation to the total variance of the daily PM model predictions over the whole study period, as commonly reported for LUR models.

3. Results

The descriptive statistical measures of the mean daily and hourly PM_{10} and $PM_{2.5}$ concentrations as observed by AQM stations that are located in four major cities of Israel are presented in Table 1. The mean daily and the hourly values measurements for the study period (2005–2015) ranged between 44 and 63 μg/m^3 for PM_{10} and 18–25 μg/m^3 for $PM_{2.5}$. The mean and median PM_{10} concentrations during the Aqua and Terra overpass times were higher by 1–7 μg/m^3 than the daily mean and median. The differences in mean and median $PM_{2.5}$ concentrations between the three time windows studied in this work ranged between 1 and 3 μg/m^3, with the highest average concentrations usually measured during the Aqua (H_A) and Terra (H_T) daytime overpass.

The CV performance measures of the daily and intra-daily $PM_{2.5}$ and PM_{10} stage 1 models for all the period (2005–2015) are summarized in

Table 2
Cross-validated performance measures of the daily and intra-daily $PM_{2.5}$ and PM_{10} stage 1 models (including the local stage).

	PM_{10}			$PM_{2.5}$		
	Daily (Aqua)	Hourly (Aqua)	Hourly (Terra)	Daily (Aqua)	Hourly (Aqua)	Hourly (Terra)
Overall R^2	0.92	0.90	0.91	0.87	0.82	0.84
Overall RMSE	19.94	30.75	24.77	6.16	8.88	9.51
Slope	1.09	1.07	1.00	1.05	1.02	1.01
Spatial R^2	0.95	0.84	0.97	0.95	0.94	0.79
Spatial RMSE	2.99	12.02	1.72	0.85	0.74	1.65
Temporal R^2	0.89	0.86	0.91	0.87	0.82	0.84
Temporal RMSE	19.88	35.29	24.72	6.14	8.86	9.46

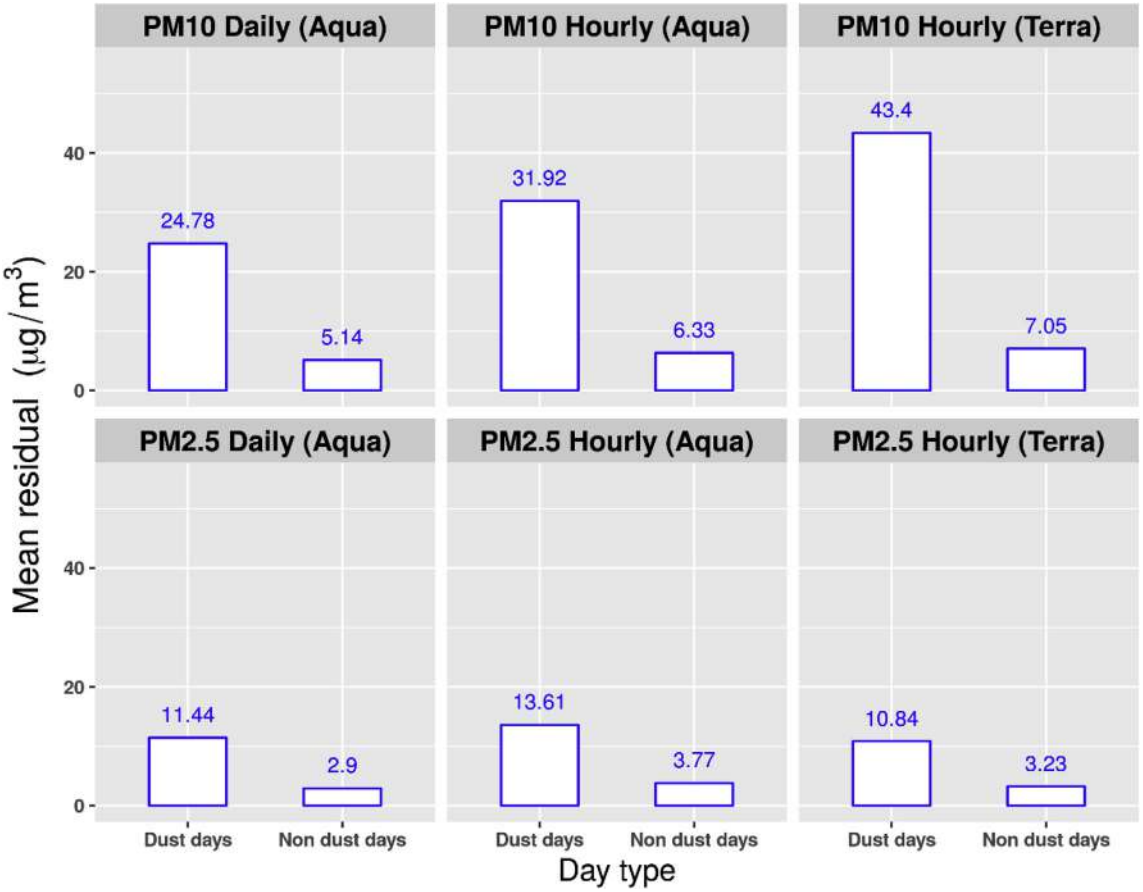

Fig. 3. The mean residual of PM_{10} and $PM_{2.5}$ predictions for each of the models in dust days and non-dust days. The mean residual was calculated as the mean of the absolute difference between the observed PM values from the air quality monitoring station and the model predicted PM values at the closet grid point.

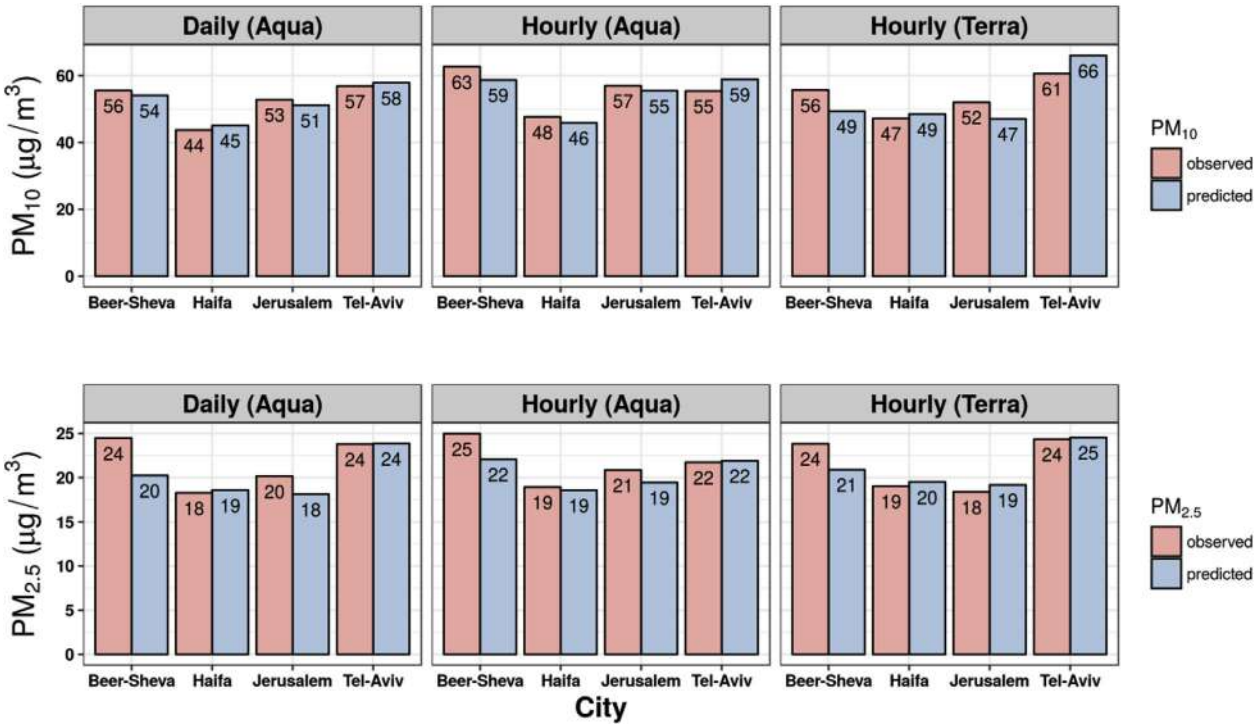

Fig. 4. Comparison of the mean daily and intra-daily observed and predicted values of particulate matter (PM) in four large cities in Israel located in different geographical areas. The mean observed values were calculated from one ground monitor in each city, while the predicted values were extracted from the closest grid cell of the model.

Table 2. All models showed good performance after applying the local stage with CV R^2 higher than 0.82 and 0.90 for the $PM_{2.5}$ and the PM_{10} models, respectively. Before applying the local stage the overall R^2 ranged between 0.79 and 0.88 for the PM_{10} models and 0.73–0.79 for the $PM_{2.5}$ models. The overall and the temporal R^2 and RMSE measures showed slightly better performance (higher R^2 and lower RMSE) for the daily models in comparison to the hourly models. However, hourly models showed slope closer to 1.00, indicating on a smaller bias. The CV overall R^2 and RMSE results for each year separately are detailed in the electronic Supplementary Material in Table A.1. The residuals of the model were calculated for non-dust (days in which dust events were not detected in any station) and dust days, separately, as the absolute difference between observed and predicted values. The mean residuals for non-dust and dust days are presented in Fig. 3 revealing that the mean residuals were up to 6 times higher in days with dust events than in non-dust days for both PM_{10} and for $PM_{2.5}$. Moreover, the highest mean

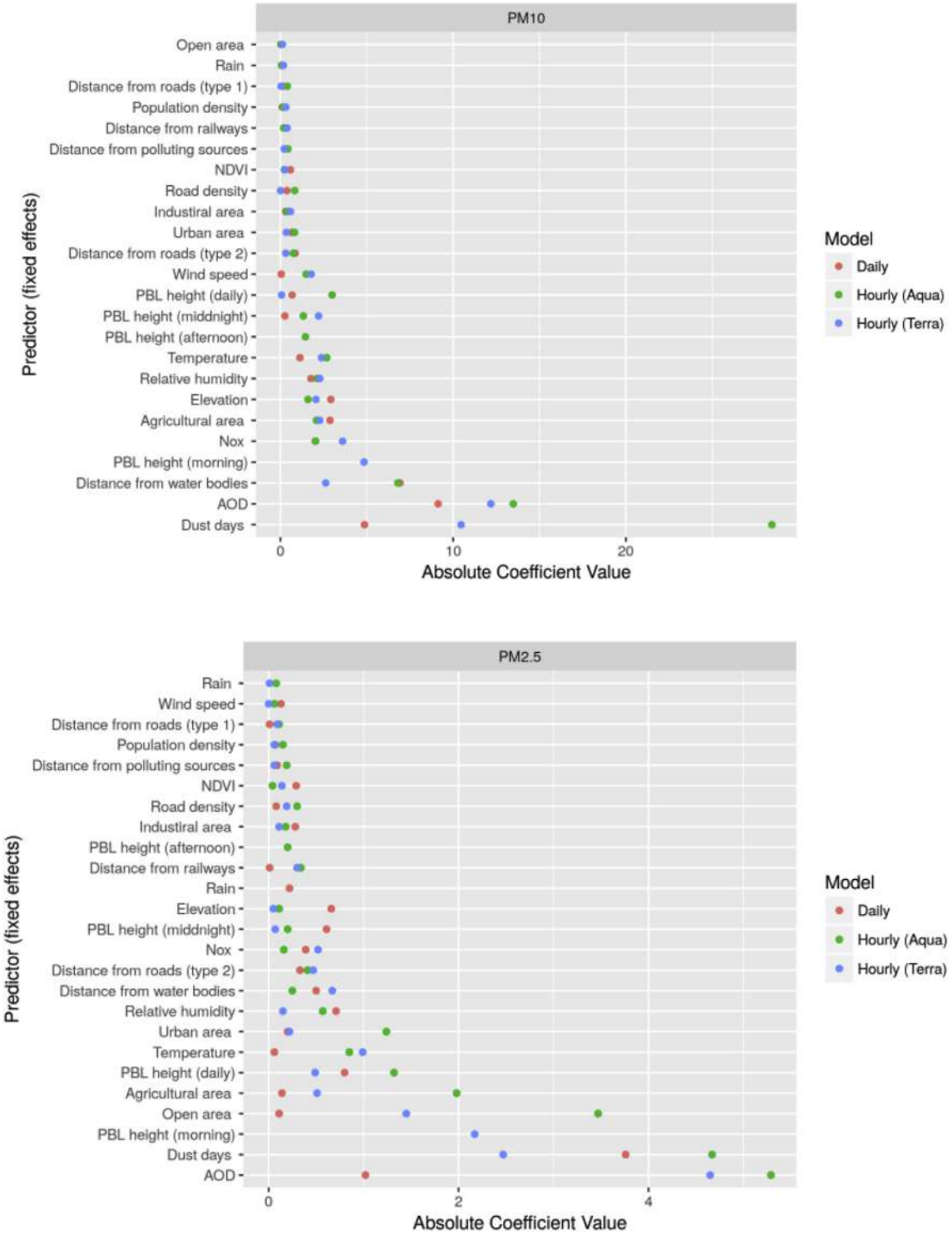

Fig. 5. The coefficients of the different spatial and temporal predictors (fixed effects). Note that the predictors were standardized and the absolute value of their coefficients was shown in this figure, therefore there is no practical interpretation to these coefficients. The values in this figure represent the relative influence of a certain fixed effect predictor in each model.

residuals were observed in the hourly models.

The mean observed and predicted daily and intra-daily $PM_{2.5}$ and PM_{10} concentrations in four large Israeli cities are presented in Fig. 4. These populated locations are examples for locations that might be of interest for epidemiological studies. The highest mean $PM_{2.5}$ and PM_{10} values were observed in Beer-Sheva and Tel-Aviv. The daily and hourly mean values for these two cities were close to 25 μg/m^3 for $PM_{2.5}$ and above 55 μg/m^3 for PM_{10}, which are higher than the guideline level defined by the World Health Organization (WHO) and the Israeli MOEP. Haifa showed the lowest mean $PM_{2.5}$ (18–19 μg/m^3) and PM_{10} concentrations (44–48 μg/m^3). The measured and predicted $PM_{2.5}$ concentrations showed differences that ranged from 1-4 μg/m^3 between the mean daily and the mean satellite overpass values, and in most cases slightly higher values were observed during the overpass of Terra or Aqua. PM_{10} concentrations were higher in the overpass time of the Aqua satellite in all the cities except for Tel-Aviv, which showed higher values during the overpass of the Terra satellite. The hybrid model showed similar mean values in most cases (Tel-Aviv, Haifa, and Jerusalem), with 1–2 μg/m^3 deviation from the measured values for $PM_{2.5}$ and 1–5 μg/m^3 for PM_{10}. The highest deviation of the model from the measured mean values was found in the Beer-Sheva, where a difference of 3–4 μg/m^3 for the $PM_{2.5}$ model and 2–7 μg/m^3 for PM_{10} model were obtained.

Fig. 5 shows the absolute coefficient values of the standardized fixed effects from the first calibration stage (mixed effects model) that includes all spatial and temporal predictors. All the fixed effects of the

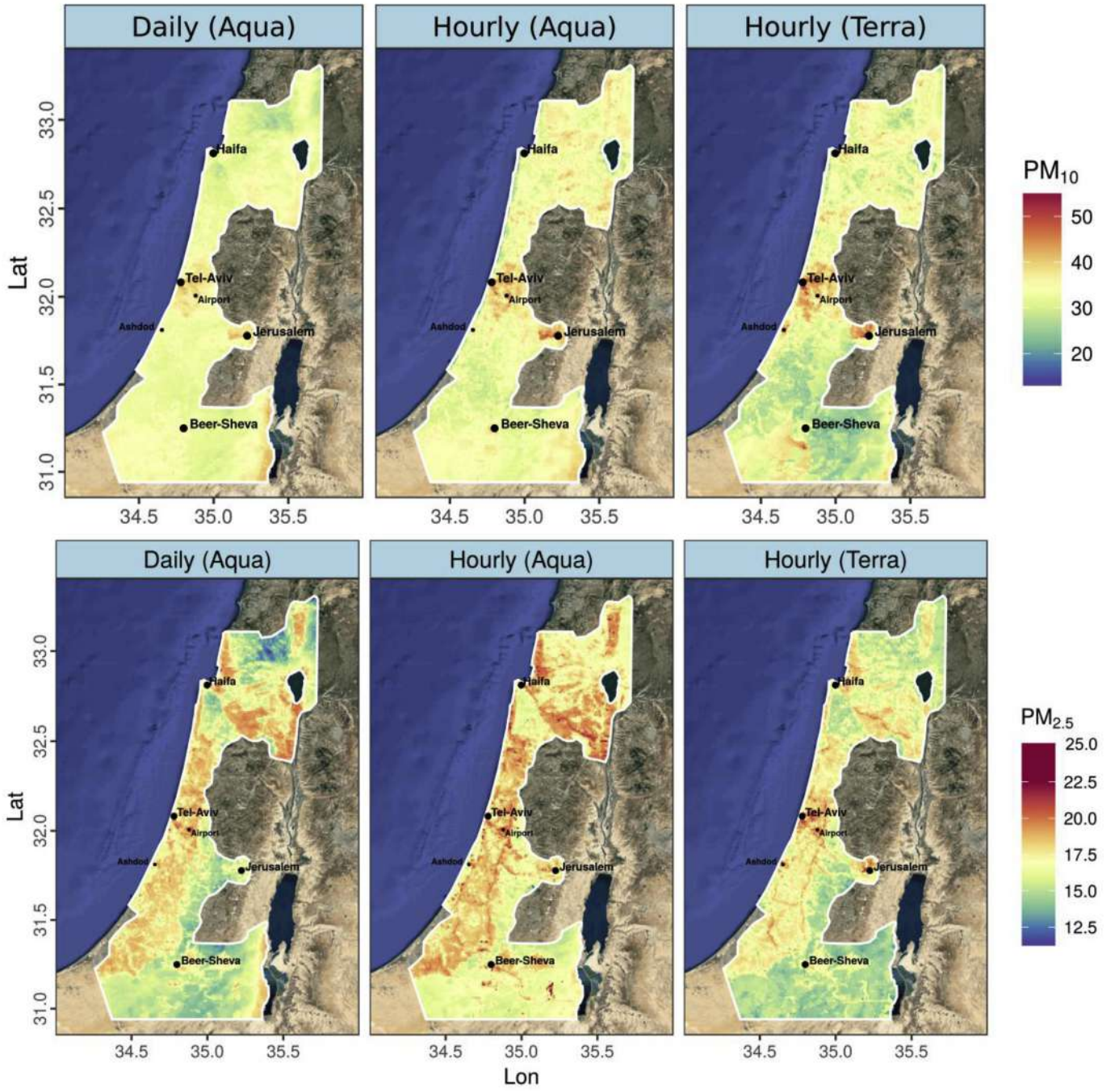

Fig. 6. Maps of the mean 2005–2015 non-dust PM_{10} and $PM_{2.5}$ model results for the three time windows: Terra overpass, Aqua overpass, and daily average (24 h mean).

Table 3
Summary statistics of the mean prediction of PM_{10} and $PM_{2.5}$ during non-dust days in 2005–2015 for the three modeled time windows. Abbreviations: Sd-standard deviation, 1st Qr., 3st Qr.- the first (25%) and the third (75%) quartiles.

	$PM_{2.5}$			PM_{10}		
	Daily (Aqua)	Hourly (Aqua)	Hourly (Terra)	Daily (Aqua)	Hourly (Aqua)	Hourly (Terra)
Mean	16.62	17.50	16.27	33.13	34.1	31.97
Sd	1.67	1.29	1.45	2.42	3.1	4.61
Median	16.54	17.34	16.09	32.82	34.1	31.77
Minimum	11.14	12.19	12.91	24.22	13.6	15.69
Maximum	21.24	24.89	22.55	44.66	51.4	55.98
1st Qr.	15.29	16.40	15.03	31.64	32.1	28.74
3st Qr.	18.1	18.56	17.47	34.44	35.8	34.76

model were standardized by subtracting their mean and dividing by their standard deviation. In all models the AOD and dust day classification were the variables with the highest absolute coefficient among the fixed effects, meaning that their relative influence on the model was the highest. It is important to note that the relation between AOD and PM is captured also as a random effect (day-specific random effect) in the model therefore this figure presents the relative influence of the fixed AOD effect.

Mean $PM_{2.5}$ and PM_{10} values in non-dust days over the whole study period for the three models' time windows are presented in Fig. 6. The spatial pattern of the mean non-dust $PM_{2.5}$ and PM_{10} over the study period (2005–2015) enables identification of more polluted areas during these days. Dust days were excluded from this analysis since the variability during dust events represents the transboundary-scale phenomena rather than the local spatial scale (Yuval et al., 2015). Moreover, for regulation purposes, the non-dust days PM concentrations are more relevant, as they reflect emissions from local sources (such as vehicles and industry) that might be reduced by regulations. The highest non-dust $PM_{2.5}$ values in Israel are found in the more populated and industrial areas. Some examples of such locations are the area around the Ben-Gurion international airport and industrial areas in Tel-Aviv, Haifa, Ashdod, and in some industrial locations in the Negev with mean 2005–2015 values that exceed 19 $\mu g/m^3$. The spatial patterns of the non-dust daily and hourly model results are generally similar, yet some differences are observed in the hourly $PM_{2.5}$ models (Fig. 6). During these time windows higher concentrations are evident around railways and in specific locations (for example in the Tel-Aviv area and around Ashdod and in some industrial locations). The spatial mean PM_{10} pattern shows that the highest concentrations during non-dust days are expected in and around Tel-Aviv and Jerusalem. During the Terra overpass, two other locations are prominent (Fig. 6, Hourly (Terra)): Ashdod and an industrial area south of Beer-Sheva. The descriptive statistics of the predicted mean PM_{10} and $PM_{2.5}$ for the period of 2005–2015 are presented in Table 3. The highest mean and median values are predicted during the Aqua overpass.

4. Discussion

$PM_{2.5}$ and PM_{10} concentrations at a resolution of 1 × 1 km across Israel were estimated for three different time windows in each day; during the overpass of Terra (mean PM between 8:00–14:00), during the overpass of Aqua (mean PM between 10:00–16:00), and over the whole day (24-hours mean). The current work extends previous work that applied the hybrid modeling approach in Israel and estimated $PM_{2.5}$ and PM_{10} on a daily level (Kloog et al., 2015) using the MAIAC AOD product. Monitoring stations in four major Israeli cities showed that in most cases the highest PM_{10} and $PM_{2.5}$ mean and median concentrations were observed during the overpass of Aqua or Terra, compared to the daily average (Table 1). The intra-daily PM estimations can be used in future epidemiology research for studying the association between these exposures and temporally resolved health outcomes which become recently more available in Israel (e.g. records from emergency rooms). Estimation of PM concentrations during different times of the day might express the diurnal variability in PM that can possibly have different sources, chemical composition, and size distribution. The temporally and spatially resolved exposure data will allow testing whether there is a different association between such health outcomes and exposure to PM concentrations in different time windows (daily and intra-daily).

Spatial maps of PM_{10} and $PM_{2.5}$ estimates during non-dust time periods (Fig. 6) show higher concentrations in populated areas, known to be characterized by increased anthropogenic pollutant emitting activities (transportation, industry). Mean PM_{10} and $PM_{2.5}$ levels during non-dust days show different spatial patterns in the three modeled time windows. For example, the hourly $PM_{2.5}$ models showed higher concentrations around railways and PM_{10} concentrations showed higher values around specific industrial areas during the Terra overpass. These patterns might suggest that some sources may be more prominent during specific times of the day. This might help focusing efforts towards anthropogenic PM emission reduction at locations that showed higher mean concentrations.

The performance of the daily models were slightly better than that of the intra-daily models (Table 2), showing lower RMSE and higher R^2. This implies that estimating highly temporally resolved PM concentrations is challenging, and potentially other temporal predictors that currently are unavailable should be taken into account in future models for improved predictions. Four large cities that are located in different geo-climatic regions were chosen for local evaluation of model performance. A comparison of mean measured and predicted PM in these cities shows that the largest deviation of the model was found in the southern city of Beer-Sheva. The lower performance of the model in this area can be due to several reasons. First, there are only few AQM stations in the southern part of Israel. Hence, relatively small amount of PM data was available for model calibration (e.g. only one $PM_{2.5}$ monitor operates in Beer-Sheva since 2011 and one PM_{10} monitor that operates since 2000). In comparison, the other cities used in this work (Tel-Aviv, Haifa, Jerusalem) have considerably more AQM stations (Fig. 1) that have been operating for a longer period. Consequently, this spread of PM monitors and the availability of observations resulted in model calibration based on relationships between PM observations and model predictors from areas that have different geo-climatic conditions than Beer-Sheva. Moreover, the PM levels in Beer- Sheva are influenced from the occurrence of dust storms more than other cities in Israel (Krasnov et al., 2016a) due to its proximity to dust emission sources.

A limitation of our model is a worse estimation of PM concentrations during days with dust storms (Fig. 4); probably due to insensitivity of the AOD to the very high aerosols loading in the atmosphere, and the fact that most of the days in the training dataset were non-dust days in which PM concentrations do not reach such high values. Dust events increase the concentration of coarser particles in the range of 2.5–10 μm (Krasnov et al., 2015). This might explain the higher PM_{10} residuals that are obtained during dust days in comparison to $PM_{2.5}$. During the last years Israel experienced several intensive dust storms that showed daily mean PM_{10} concentrations of 2000–3000 $\mu g/m^3$ in several monitors during storms in 2006, 2007, 2010, and 2012, and even above 3000 $\mu g/m^3$ daily PM_{10} during the September 2015 dust storm. The frequency of dust storms in this area is increasing in the last decade (Krasnov et al., 2016a), and associations between these extreme events and different health outcomes were documented (Vodonos et al., 2016, 2014). Future work may overcome on the current limitation by either adding a dust storm classification predictor that refers to the severity of the dust storm, or fitting a separate model for days affected by dust storms.

5. Conclusions

Estimation of PM_{10} and $PM_{2.5}$ in Israel on a daily and intra-daily temporal resolution around the overpass of the two satellite platforms of the MODIS sensor (Terra and Aqua) showed different spatial pattern of the mean PM for non-dust period (days not affected by dust storms). During the overpass times of Terra and Aqua some areas in Israel showed higher PM concentrations relative to the mean daily spatial pattern. These estimations can be used for regulatory purposes and help focusing pollution reduction efforts to specific areas that were spotted as suffering from increased levels using the model. Israel is a complex domain for PM modeling due to its various geo-climatic conditions and natural and anthropogenic sources of PM. Nonetheless, the hybrid model performed well showing overall R^2 that ranged between 0.82 and 0.92. The lower performance of the intra-daily models in comparison to the daily average models indicates a bigger challenge to estimate PM concentrations in fine temporal resolution. The model showed higher residuals in days that experienced dust storms, and usually underestimated PM levels during such days.

Declarations of interest

None.

Acknowledgments

This work was supported by a research grant [grant number: 3-13142] from of the Ministry of Science and Technology. The author would like to thank the Ministry of Science and Technology, Israel for the supporting the research and A.S with a PhD scholarship. The authors would also like to thank the Technion Center of Excellence in Exposure Science and Environmental Health (TCEEH) for maintaining and providing the air pollution and meteorological database.

Appendix A. Supplementary data

Supplementary data related to this article can be found at https://doi.org/10.1016/j.atmosenv.2018.08.002.

References

Arvani, B., Pierce, R.B., Lyapustin, A.I., Wang, Y., Ghermandi, G., Teggi, S., 2016. Seasonal monitoring and estimation of regional aerosol distribution over Po valley, northern Italy, using a high-resolution MAIAC product. Atmos. Environ. 141, 106–121. https://doi.org/10.1016/j.atmosenv.2016.06.037.

ASTER, 2014. ASTER Global Digital Elevation Map. https://asterweb.jpl.nasa.gov/gdem.asp.

Bates, D., Mächler, M., Bolker, B., Walker, S., 2015. Fitting linear mixed-effects models using lme4. J. Stat. Software 67, 51. https://doi.org/10.18637/jss.v067.i01.

Bell, M.L., Ebisu, K., Belanger, K., 2007. Ambient air pollution and low birth weight in Connecticut and Massachusetts. Environ. Health Perspect. 115, 1118–1124. https://doi.org/10.1289/ehp.9759.

Chudnovsky, A.A., Koutrakis, P., Kloog, I., Melly, S., Nordio, F., Lyapustin, A., Wang, Y., Schwartz, J., 2014. Fine particulate matter predictions using high resolution Aerosol Optical Depth (AOD) retrievals. Atmos. Environ. 89, 189–198. https://doi.org/10.1016/j.atmosenv.2014.02.019.

D'Ippoliti, D., Forastiere, F., Ancona, C., Agabiti, N., Fusco, D., Carlo, A.P., 2003. Air pollution and myocardial infarction in Rome analysis a case-crossover. Epidemiology 14, 528–535. https://doi.org/10.1097/01.ede.0000082046.22919.72.

de Hoogh, K., Stafoggia, M., Künzli, N., Kloog, I., 2018. Modelling daily PM 2.5 concentrations at high spatio-temporal resolution across Switzerland. Environ. Pollut. 233, 1147–1154. https://doi.org/10.1016/j.envpol.2017.10.025.

Derimian, Y., Karnieli, A., Kaufman, Y.J., Andreae, M.O., Andreae, T.W., Dubovik, O., Maenhaut, W., Koren, I., Holben, B.N., 2006. Dust and pollution aerosols over the Negev desert, Israel: properties, transport, and radiative effect. J. Geophys. Res. Atmos. 111, 1–14. https://doi.org/10.1029/2005JD006549.

Dominici, F., Peng, R.D., Bell, M.L., Mcdermott, A., Zeger, S.L., Samet, J.M., 2006. Fine particulate air pollution and hospital admission for cardiovascular and respiratory diseases. JAMA 295, 1127–1134.

ECMWF, 2016. Modeled Planetary Boundary Layer Data. http://apps.ecmwf.int/datasets/data/interim-full-daily/levtype=sfc/, Accessed date: 5 January 2016.

EPA, 2017. Quality Assurance Handbook for Air Pollution Measurement Systems-volume II: Ambient Air Quality Monitoring Program.

ESRI, 2018. ArcGIS Desktop: Release 10.3. Redlands, CA, USA.

Falkovich, A.H., 2004. Adsorption of organic compounds pertinent to urban environments onto mineral dust particles. J. Geophys. Res. 109, D02208. https://doi.org/10.1029/2003JD003919.

Freiman, M.T., Hirshel, N., Broday, D.M., 2006. Urban-scale variability of ambient particulate matter attributes. Atmos. Environ. 40, 5670–5684. https://doi.org/10.1016/j.atmosenv.2006.04.060.

Ganor, E., Stupp, A., Alpert, P., 2009. A method to determine the effect of mineral dust aerosols on air quality. Atmos. Environ. 43, 5463–5468. https://doi.org/10.1016/j.atmosenv.2009.07.028.

GISrael, 2012. GISrael Database of MAPA. http://www.gisrael.co.il/eng, Accessed date: 1 January 2012.

Gupta, P., Christopher, S.A., 2008. Seven year particulate matter air quality assessment from surface and satellite measurements. Atmos. Chem. Phys. 8, 3311–3324.

Hartog, J.J. De, Lanki, T., Timonen, K.L., Hoek, G., Janssen, N.A.H., Ibald-mulli, A., Peters, A., Heinrich, J., Tarkiainen, T.H., Grieken, R. Van, Brunekreef, B., Pekkanen, J., 2009. Associations between PM 2.5 and heart rate variability are modified by particle composition and beta-blocker use in patients with coronary heart disease. Environ. Health Perspect. 117, 105–111. https://doi.org/10.1289/ehp.11062.

Hu, X., Waller, L.A., Lyapustin, A., Wang, Y., Al-Hamdan, M.Z., Crosson, W.L., Estes, M.G., Estes, S.M., Quattrochi, D.A., Puttaswamy, S.J., Liu, Y., 2014. Estimating ground-level PM2.5 concentrations in the Southeastern United States using MAIAC AOD retrievals and a two-stage model. Remote Sens. Environ. 140, 220–232. https://doi.org/10.1016/j.rse.2013.08.032.

ICBS, 2016. Central Bureau of Statistics. http://www.cbs.gov.il/reader/?MIval=cw_usr_view_Folder&ID=141.

Jerrett, M., Arain, A., Kanaroglou, P., Beckerman, B., Potoglou, D., Sahsuvaroglu, T., Morrison, J., Giovis, C., 2005. A review and evaluation of intraurban air pollution exposure models. J. Expo. Anal. Environ. Epidemiol. 15, 185–204. https://doi.org/10.1038/sj.jea.7500388.

Just, A.C., Wright, R.O., Schwartz, J., Coull, B.A., Baccarelli, A., Tellez-rojo, M.M., Moody, E., Wang, Y., Lyapustin, A., Kloog, I., 2015. Using High-resolution Satellite Aerosol Optical Depth to Estimate Daily $PM_{2.5}$ Geographical Distribution in Mexico City. https://doi.org/10.1021/acs.est.5b00859.

Karnieli, A., Derimian, Y., Indoitu, R., Panov, N., Levy, R.C., Remer, L.A., Maenhaut, W., Holben, B.N., 2009. Temporal trend in anthropogenic sulfur aerosol transport from central and eastern Europe to Israel. J. Geophys. Res. Atmos. 114. https://doi.org/10.1029/2009JD011870.

Katra, I., Arotsker, L., Krasnov, H., Zaritsky, A., Kushmaro, A., Ben-Dov, E., 2014. Richness and diversity in dust stormborne biomes at the southeast mediterranean. Sci. Rep. 4, 19–24. https://doi.org/10.1038/srep05265.

Katra, I., Elperin, T., Fominykh, A., Krasovitov, B., Yizhaq, H., 2016. Modeling of particulate matter transport in atmospheric boundary layer following dust emission from source areas. Aeolian Res 20, 147–156. https://doi.org/10.1016/j.aeolia.2015.12.004.

Kloog, I., Coull, B.A., Zanobetti, A., Koutrakis, P., Schwartz, J.D., 2012a. Acute and chronic effects of particles on hospital admissions in new-England. PLoS One 7, 2–9. https://doi.org/10.1371/journal.pone.0034664.

Kloog, I., Melly, S.J., Ridgway, W.L., Coull, B.A., Schwartz, J., 2012b. Using new satellite based exposure methods to study the association between pregnancy pm 2.5 exposure, premature birth and birth weight in Massachusetts. Environ. Health 11, 1–8.

Kloog, I., Ridgway, B., Koutrakis, P., Coull, B.A., Schwartz, J.D., Program, R., 2013. Long- and short-term exposure to PM2.5 and mortality: using novel exposure models. Epidemiology 24, 555–561. https://doi.org/10.1097/EDE.0b013e318294beaa.

Kloog, I., Sorek-hamer, M., Lyapustin, A., Coull, B., Wang, Y., Just, A.C., Schwartz, J., Broday, D.M., 2015. Estimating daily PM 2.5 and PM 10 across the complex geo-climate region of Israel using MAIAC satellite-based AOD data. Atmos. Environ. 122, 409–416. https://doi.org/10.1016/j.atmosenv.2015.10.004.

Kok, J.F., 2011. Does the size distribution of mineral dust aerosols depend on the wind speed at emission? Atmos. Chem. Phys. 11, 10149–10156. https://doi.org/10.5194/acp-11-10149-2011.

Krasnov, H., Katra, I., Friger, M., 2016a. Increase in dust storm related PM10concentrations: a time series analysis of 2001-2015. Environ. Pollut. 213, 36–42. https://doi.org/10.1016/j.envpol.2015.10.021.

Krasnov, H., Katra, I., Koutrakis, P., Friger, M.D., 2014. Contribution of dust storms to PM10 levels in an urban arid environment. J. Air Waste Manag. Assoc. 64, 89–94. https://doi.org/10.1080/10962247.2013.841599.

Krasnov, H., Katra, I., Novack, V., Vodonos, A., Friger, M.D., 2015. Increased indoor PM concentrations controlled by atmospheric dust events and urban factors. Build. Environ. 87, 169–176. https://doi.org/10.1016/j.buildenv.2015.01.035.

Krasnov, H., Kloog, I., Friger, M., Katra, I., 2016b. The spatio-temporal distribution of particulate matter during natural dust episodes at an urban scale. PLoS One 11, 5–9. https://doi.org/10.1371/journal.pone.0160800.

Kurt, S., Cohen, A., Samet, J.M., 2013. Air Pollution and Cancer. IARC scientific publications. International Agency for Research on Cancer, Lyon. https://doi.org/10.1007/s13398-014-0173-7.2.

Lee, M., Kloog, I., Chudnovsky, A., Lyapustin, A., Wang, Y., Melly, S., Coull, B., Koutrakis, P., Schwartz, J., 2015. Spatiotemporal prediction of fi ne particulate matter using high-resolution satellite images in the Southeastern US 2003 – 2011. J. Expo. Sci. Environ. Epidemiol. 1–8. https://doi.org/10.1038/jes.2015.41.

Levy, I., Levin, N., Yuval, Schwartz, J.D., Kark, J.D., 2015. Back-extrapolating a land use regression model for estimating past exposures to traffic-related air pollution. Environ. Sci. Technol. 49, 3603–3610. https://doi.org/10.1021/es505707e.

Li, S., Joseph, E., Min, Q., Yin, B., Sakai, R., Payne, M.K., 2017. Remote sensing of PM2.5 during cloudy & nighttime periods using ceilometer backscatter. Atmos. Meas. Tech. 10, 2093–2104. https://doi.org/10.5194/amt-10-2093-2017.

Lyapustin, A., Martonchik, J., Wang, Y., Laszlo, I., Korkin, S., 2011a. Multiangle implementation of atmospheric correction (MAIAC): 1. Radiative transfer basis and look - up tables. J. Geophys. Res. 116. https://doi.org/10.1029/2010JD014985.

Lyapustin, A., Wang, Y., Laszlo, I., Kahn, R., Korkin, S., Remer, L., Levy, R., Reid, J.S., 2011b. Multiangle implementation of atmospheric correction (MAIAC): 2. Aerosol algorithm. J. Geophys. Res. 116, 1–15. https://doi.org/10.1029/2010JD014986.

Madrigano, J., Kloog, I., Goldberg, R., Coull, B.A., Mittleman, M.A., 2013. Long-term exposure to PM 2.5 and incidence of acute myocardial infarction. Environ. Health Perspect. 192, 192–196.

MEP, 2018. EPA. http://www.sviva.gov.il/subjectsEnv/SvivaAir/Laws/Pages/toxicityvalue.aspx, Accessed date: 4 January 2018.

Meyer, D., Dimitriadou, E., Hornik, K., Weingessel, A., Leisch, F., 2017. e1071: Misc Functions of the Department of Statistics. Probability Theory Group (Formerly: E1071).

Oke, T.R., 1987. Boundry Layer Climates. Psychology Press.

R, 2017. R: a Language and Environment for Statistical Computing, Vienna, Austria.

Rich, D.Q., Halu, O., Crooks, J., Baxter, L., Burke, J., Ohman-strickland, P., Thevenet-morrison, K., Kipen, H.M., Zhang, J., Kostis, J.B., Lunden, M., Hodas, N., Turpin, B.J., 2013. The triggering of myocardial infarction by fine particles is enhanced when particles are enriched in secondary species. Environ. Sci. Technol. 47, 9414–9423.

Schwartz, J., 1995. Air pollution and hospital admissions for respiratory disease. Epidemiology 7, 20–28.

Sorek-hamer, M., Kloog, I., Just, A.C., 2016. Satellite remote sensing in epidemiological studies Satellite remote sensing in epidemiological studies. Curr. Opin. Pediatr. 27. https://doi.org/10.1097/MOP.0000000000000326.

Stafoggia, M., Schwartz, J., Badaloni, C., Bellander, T., Alessandrini, E., Cattani, G., de' Donato, F., Gaeta, A., Leone, G., Lyapustin, A., Sorek-Hamer, M., de Hoogh, K., Di, Q., Forastiere, F., Kloog, I., 2016. Estimation of daily PM 10 concentrations in Italy (2006-2012) using finely resolved satellite data, land use variables and meteorology. Environ. Int. 99, 1–49. https://doi.org/10.1016/j.envint.2016.11.024.

Tremblay, A., Ransijn, J., 2015. LMERConvenienceFunctions: Model Selection and Post-hoc Analysis for (G)LMER Models.

Uzan, L., Egert, S., Alpert, P., 2012. The coastal boundary layer and air pollution - a high temporal resolution analysis in the east mediterranean coast. Open Atmos. Sci. J. 6, 9–18.

Vodonos, A., Friger, M., Katra, I., Avnon, L., Krasnov, H., Koutrakis, P., Schwartz, J., Lior, O., Novack, V., 2014. The impact of desert dust exposures on hospitalizations due to exacerbation of chronic obstructive pulmonary disease. Air Qual. Atmos. Heal. 7, 433–439. https://doi.org/10.1007/s11869-014-0253-z.

Vodonos, A., Kloog, I., Boehm, L., Novack, V., 2016. The impact of exposure to particulate air pollution from non-Anthropogenic sources on hospital admissions due to pneumonia. Eur. Respir. J. 48, 1791–1794. https://doi.org/10.1183/13993003.01104-2016.

You, W., Zang, Z., Zhang, L., Li, Y., Pan, X., Wang, W., 2016. National-scale estimates of ground-level PM2.5 concentration in China using geographically weighted regression based on 3 km resolution MODIS AOD. Rem. Sens. 8. https://doi.org/10.3390/rs8030184.

Yuval, Sorek-Hamer, M., Stupp, A., Alpert, P., Broday, D.M., 2015. Characteristics of the east Mediterranean dust variability on small spatial and temporal scales. Atmos. Environ. 120, 51–60. https://doi.org/10.1016/j.atmosenv.2015.08.058.

Zanobetti, A., Schwartz, J., 2005. The effect of particulate air pollution on emergency admissions for myocardial Infarction : a multicity case-crossover analysis. Environ. Health Perspect. 978, 978–982. https://doi.org/10.1289/ehp.7550.

Zeka, A., Melly, S.J., Schwartz, J., 2008. The effects of socioeconomic status and indices of physical Massachusetts. Environ. Health 7, 1–13. https://doi.org/10.1186/1476-069X-7-60.

Zikova, N., Masiol, M., Chalupa, D., Rich, D., Ferro, A., Hopke, P., 2017. Estimating hourly concentrations of PM2.5 across a metropolitan area using low-cost particle monitors. Sensors 17, 1922. https://doi.org/10.3390/s17081922.